Coherence Length Characteristics from Broadband Semiconductor Emitters: Superluminescent Diodes versus Broadband Laser Diodes

C. E. Dimas[a], C. L. Tan[a], H. S. Djie[b], B. S. Ooi[a*]

[a]Center for Optical Technologies and Department of Electrical and Computer Engineering, Lehigh University, 7 Asa Drive, Bethlehem, PA, USA 18015;
[b]JDS Uniphase Corporation, San Jose, CA, USA 95134;
*corresponding author: bsooi@ieee.org

ABSTRACT

This paper reports on the measurement and analysis of the coherence function for broadband emitters such as superluminescent diodes (SLDs) and novel broadband laser diodes (BLDs) from self-assembled InGaAs/GaAs quantum-dot (QD) and InAs/InP quantum-dash (Qdash) structures that emit at center wavelengths of 1150nm and 1650nm, respectively. Using the fiber-based spectral interferometry system, coherence lengths in fiber of 23 μm and 48 μm have been measured from the QD and Qdash BLDs. Larger spectral bandwidth of 137 nm and 78 nm have been measured from the QD and Qdash SLDs that yield coherence lengths in fiber of 3 μm and 10 μm, respectively. The coherence function of both BLDs and SLD reveals negligible secondary coherence subpeaks and sidelobes indicating the possibility of using these broadband sources to produce low artifacts optical coherence tomography (OCT) images.

Keywords: Coherence length, optical coherence tomography, semiconductor laser, quantum-dash, quantum-dot, superluminescent diode

1. INTRODUCTION

Broad spectral bandwidth sources in the near-infrared (NIR) wavelength regime are highly desirable for sensing and imaging systems based on low coherent interferometry such as optical coherence tomography (OCT) [1,2]. In an OCT system, broad spectral bandwidth light source emitting at high optical power is required to increase the axial resolution and to improve the sensitivity of the system [1,2]. Semiconductor light sources such as superluminescent diodes (SLDs) and broadband lasers (BLDs) are compact light sources with broad spectral bandwidth and high optical power. SLDs have laser-like characteristics of high power and low beam divergence while having a broad amplified spontaneous emission spectrum which is several folds larger than stimulated emission from typical lasers [3-8]. Recently developed, BLDs are a new class of semiconductor lasers which have 100 times wider spectral width than typical laser diodes [8-11]. Emitters with active regions of quantum-dots (QDs) and quantum-dashes (Qdashes) were postulated to yield wider spectral bandwidths, high optical gain and improved temperature sensitivity beyond quantum wells capabilities [12]. SLDs and BLDs based on QD/Qdash have demonstrated to be compact broad spectral bandwidth and high emission power light sources highly favorable for low coherent interferometry applications [5-11]. The broad, continuous emission spectra from these light sources can be obtained by engineering the optical gain characteristics in the naturally inhomogeneous QD/Qdash media to produce an overlap emission from multiple quantum confined states. In addition, the characteristic Gaussian-like low ripple emission from these devices makes them particularly attractive for OCT than other bulky alternative broadband sources [2]. Spectral deviations such as significant spectral dips and modulations of the source emissions can cause image artifacts and masking can result from [13].

While there have been many reports utilizing an optical spectrum analyzer to characterize broadband light sources, the important corresponding temporal coherence function from these emitters, which impacts resolution, signal quality and noise levels in OCT, is still understudied. So far, only few measurements of the coherence function of SLDs have been reported [4,7]. In this paper, we report the first measurement of the temporal coherence function in InGaAs/GaAs QD based SLDs, novel InGaAs/GaAs QD BLDs as well as recently developed InAs/InGaAlAs Qdash BLDs.

Novel In-Plane Semiconductor Lasers VIII, edited by Alexey A. Belyanin, Peter M. Smowton,
Proc. of SPIE Vol. 7230, 72300B · © 2009 SPIE · CCC code: 0277-786X/09/$18 · doi: 10.1117/12.809118

2. MEASUREMENT SETUP

An optical fiber based interferometer system was setup to acquire the spectral interferogram from which the coherence length can be generated. Unlike the time-domain interferometer, the spectral interferometer does not require any moving reference mirrors. In the spectral interferometer, a single broadband depth scan encodes the origin of backscattered light relative to the distance of a parallel arm into the frequency spacing of the spectral fringes [1]. Fig. 1 shows the Fourier-domain fiber-based interferometer, which consists of a broadband source, a 2x2 single mode fiber (SMF) splitter/combiner, gold-coated mirrors, and an optical spectrum analyzer (OSA). In this system, the source is split into two paths (Arm_1 and Arm_2) that are reflected and combined in the fiber coupler. The spectral interference signal is then detected by the OSA, which has a spectral resolution set to 0.05 nm.

There are several advantages for this simple coherence measurement system. In this system, optical feedback to the light source is minimized with an AR coated tapered SMF, which couples light from the unpackaged SLD/BLD. Gold mirrors are placed in contact with Arm_1 and Arm_2 terminals to increase reflectance and to minimize dispersion of the reflected lights. As all optical waves are split/combined and confined in unstressed fiber, the split/reflected signals are reasonably expected to have equal polarization. This technique, hence, eliminates the requirement of polarization matching components.

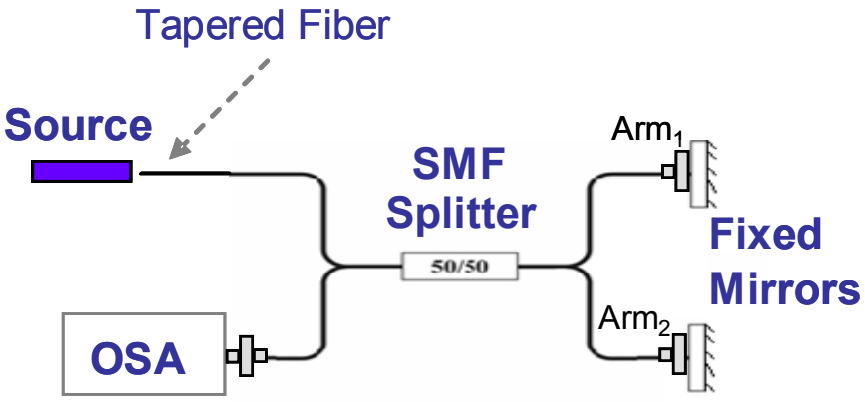

Figure 1. The schematic of fiber-based spectral interferometric system used in our experiment. This system consists of a broadband light source (either a SLD or BLD) coupled into a tapered SMF, a 2x2 fiber splitter/combiner, Arm_1 and Arm_2 that are in contact with fixed Au-coated mirrors, and an OSA for signal detection.

Since the optical pathlength difference (OPD) between Arm_1 and Arm_2 is greater than the coherence length, l_c, interference fringes are evident from a spectral interferogram, unlike a temporal domain interferogram which requires *OPD*s of much less than l_c. This can be formulated as [14]:

$$I(t) = I_1(t) + I_2(t) + 2\left|\alpha^* \gamma\right| e^{\frac{-OPD}{l_c}} \cos(\beta_o OPD) \qquad (1)$$

where I is the interference intensity; I_1, I_2 are the intensities of the optical fields of Arm_1 and Arm_2, respectively; α, γ are the coupling ratios of each arm; β_o is the propagation constant calculated at center wavelength. Equation (1) shows that the interference visibility is governed by the $exp[-OPD/l_c]$, which is the envelope of the normalized cross-correlation function between I_1 and I_2 subject to OPD. Consequently, the interference fringes will be greater if OPD > l_c in the frequency domain but diminishes in the spatial domain due to the inverse nature of the two domains [14]. If the OPD is too large, too many fringes can appear relative to the OSA resolution causing undersampling of the spectral interferogram. Hence a 2x2 fiber splitter/combiner with a proper OPD is essential in this measurement setup.

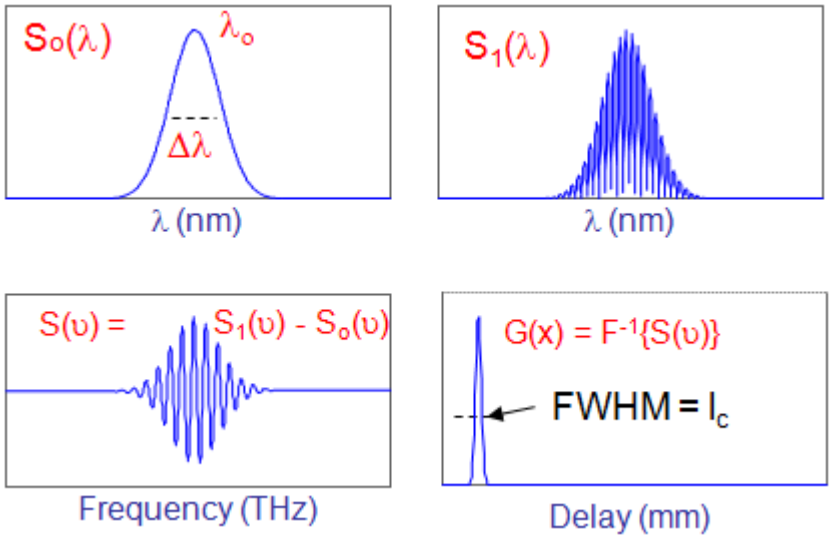

Figure 2. Ideal Gaussian simulated functions for the input, $S_o(\lambda)$, and the corresponding spectral interferogram, $S_I(\lambda)$, as well as $S(\upsilon)$, which is $S_I(\upsilon)$-$S_o(\upsilon)$ and $G(x)$, the coherence function.

The (roundtrip) coherence length, l_c, of a light source is found experimentally by measuring the full width half maximum (FWHM) of the coherence function versus distance delay. This function is generated by taking the following steps [15] which as also illustrated in Fig. 2:

i) Use the OSA to measure $S_I(\lambda)$, the spectral interferogram, and $S_o(\lambda)$, the source input spectrum
ii) Subtract $S_o(\lambda)$ from $S_I(\lambda)$
iii) Convert wavelength to evenly sampled wavenumbers via interpolation
iv) Take the inverse Fourier transform of the spectral interferogram
v) Convert wavenumber to time delay and distance delay.

For a light source with a Gaussian emission spectrum, l_c can be calculated from the following equation [1].

$$l_c = \frac{2\ln(2)}{\pi n_g}\frac{\lambda^2}{\Delta\lambda} \tag{2}$$

where λ_o is the center wavelength, $\Delta\lambda$ is the FWHM of the source and n_g is the group refractive index.

3. MATERIAL AND DEVICE DESIGN

SLDs and BLDs were fabricated from a InGaAs/GaAs QD structure with five InGaAs QD stacks and six 40 nm thick GaAs matrix layers described previously [5,9]. SLDs and BLDs were also fabricated from a Qdash-in-well active region consisting of InAs QDash embedded in InAlGaAs quantum wells (QWs) on an InP substrate as has been detailed elsewhere [6,8,10]. The SLD design (as shown in Fig. 3(a)) is composed of a 4 μm wide ridge butt-coupled to a broad area photon absorber (PA), to suppress lasing. The BLD consisted of a 50 μm stripe broad area laser.

The InGaAs/GaAs QD wafer structure (Fig. 3(a)) was grown by a molecular beam epitaxy (MBE) system on Si-doped (100)-oriented GaAs substrates. A 1500-nm-thick $Al_{0.3}Ga_{0.7}As$ lower cladding layer was first grown, which was followed by a superlattice of 20 pairs of 2-nm $Al_{0.3}Ga_{0.7}As$ and 2-nm GaAs. Five InGaAs dot layers were then consecutively grown, with each dot layer comprising of five pairs of alternating InAs and GaAs submonolayers. Under a constant arsenic flux, growth was interrupted after each monolayer in order to stabilize the surface. GaAs spacers of 40 nm thick were inserted between the QD layers. The dots formation was established and monitored by reflection high-energy electron diffraction. The bulk cladding and superlattice layers were all grown at typical (Al)GaAs substrate temperatures of 600°C, while the QD layers were grown at typical InGaAs substrate temperatures of 515°C.

The InAs/InAlGaAs Qdash wafer structure was grown by molecular beam epitaxy (MBE) on (100) oriented S-doped InP substrate. The wafer structure (Fig. 3(b)) is a p-i-n configuration with an undoped separate confinement heterostructure (SCH) waveguide design consisting of a 320-nm thick $In_{0.52}Ga_{0.28}Al_{0.2}As$ (E_g=1.0184 eV) lattice matched to an InP substrate. The lower cladding consists of an InP substrate and a 200-nm thick $In_{0.52}Al_{0.48}As$ layer doped with Si at $1 \times 10^{18}cm^{-3}$. The upper cladding and contact layers are 1700-nm-thick $In_{0.52}Al_{0.48}As$ and 150-nm-thick $In_{0.53}Ga_{0.47}As$ with Be doping of $2 \times 10^{18}cm^{-3}$, respectively. The upper cladding and capping dopant of Berillium was determined for optimal resistivity, sufficient injection current and temperature stability. In the center of the waveguide core, the dash-in-well active region, which is intentionally left undoped, has an InAs quantum-dash layer in an asymmetric InAlGaAs QW. It consists of four alternating stacks of 1.3-nm-thick compressively strained $In_{0.64}Ga_{0.16}Al_{0.2}As$ layers, a five monolayer (ML) thick InAs dash layer, and a 6.3-nm thick compressively strained $In_{0.64}Ga_{0.16}Al_{0.2}As$ layer. Each dash-in-well stack is separated by a 30-nm thick tensile-strained $In_{0.50}Ga_{0.32}Al_{0.18}As$ layer that acts as the strain-compensating barrier. The InAs quantum-dash (E_g = 0.354eV) layers were grown 1 ML at a time, each separated by 5 second growth pauses. The Qdash island formation via the coherent Stranski–Kranstanov growth mode was monitored by reflection high-energy electron diffraction. The growth temperature for the entire structure was 470°C.

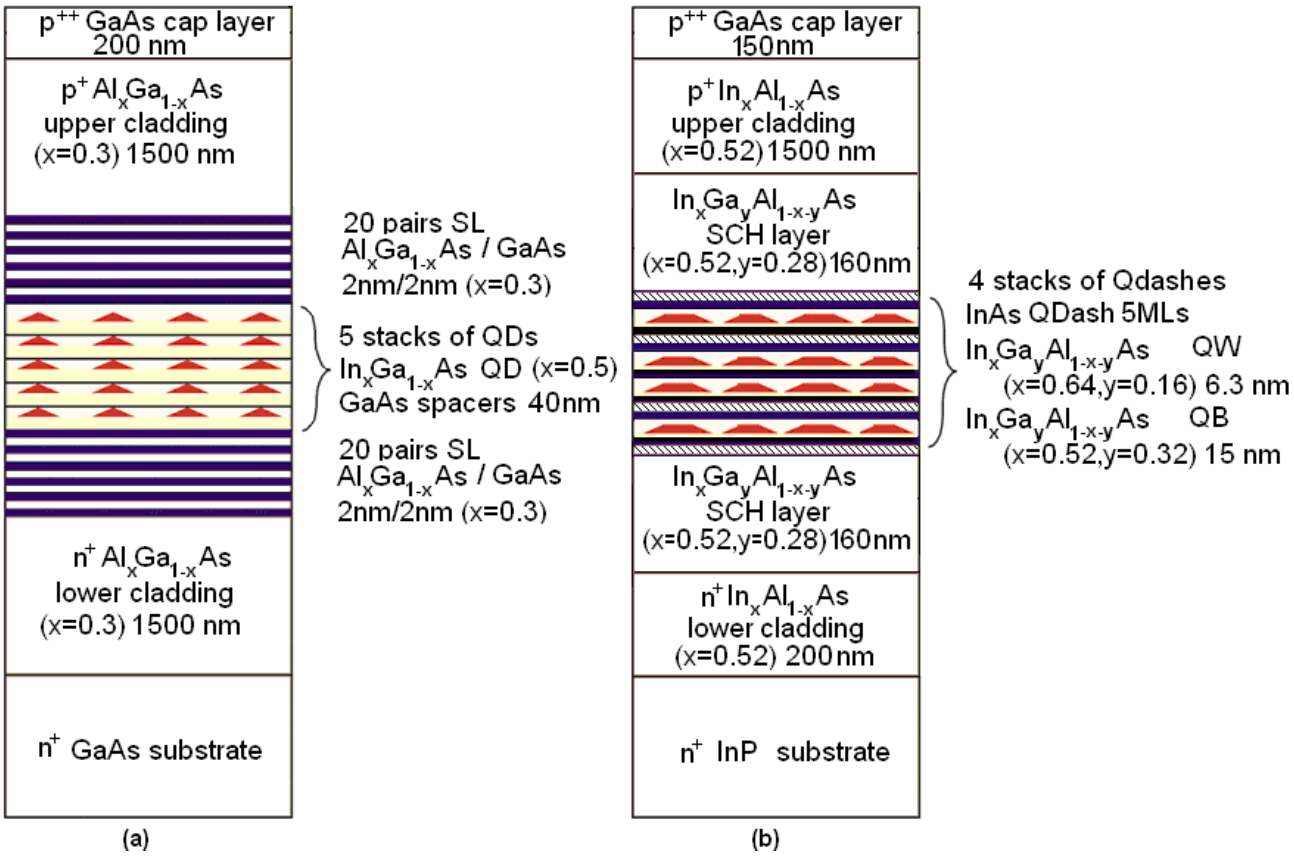

Figure 3. The InGaAs/GaAs QD (a) and the InAs/InAlGaAs Qdash (b) wafer structure composition.

4. RESULTS AND DISCUSSION

These QD and Qdash SLDs were tested at 20°C under continuous wave (CW) operation at current injections of 0.1 I_{th} and 0.4 I_{th}, respectively. The theoretical and experimental l_c in fiber for the InGaAs/GaAs QD SLD is 2.75 μm and 2.74 μm, respectively, while the calculated and measured l_c of the InAs/InGaAlAs Qdash SLD is 9.88 μm and 8.42 μm,

respectively. The l_c in air based on the measured signals is 4.00 μm and 12.29 μm, for the InGaAs/GaAs QD and InAs/InGaAlAs Qdash SLDs, respectively. The reduction of the spectral bandwidth in the InAs/InGaAlAs Qdash BLD following the calculated l_c may be attributed to the non-symmetric emission. Fig. 4 shows the coherence function versus distance delay and the inset illustrates step (*ii*), ($S_1(\lambda)$-$S_o(\lambda)$), in the data processing sequence described in the previous section. The physical pathlength difference between Arm_1 and Arm_2, l, which is defined as $l=OPD/(2n_g)$, is ~250 μm as shown in Fig. 3 at the peak of the coherence function.

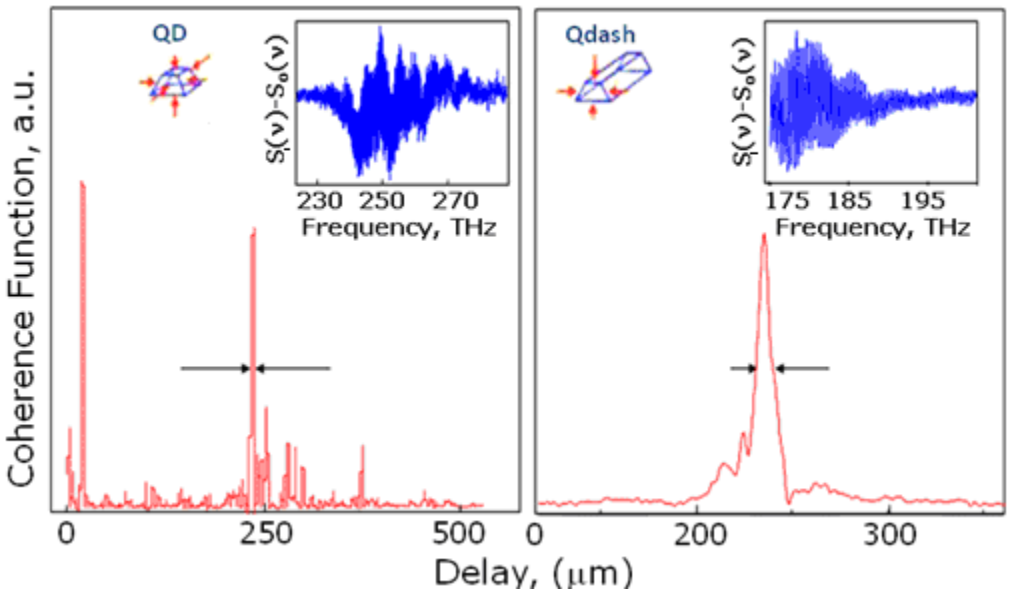

Figure 4. Temporal coherence functions of the InGaAs/GaAs QD (a) and the InAs/InGaAlAs Qdash (b) SLDs taken at 20°C. The insets delineate the intensity of the spectral interferogram minus the input versus frequency.

In addition to the coherence length, l_c, and pathlength difference of the system, the coherence function also reveals the impact of side lobes on the coherence length, l_c, and the significance of far range peaks on sensitivity. Secondary coherence subpeaks can appear in shorter range if a prominent spectral dip occurs between multiple-state excitation peaks. Since InGaAs/GaAs QD and InAs/InGaAlAs Qdash SLDs tested have small spectral dips (< 1 dB), secondary sidelobes were suppressed by more than 9 dB and 11 dB, respectively, without significantly increasing the coherence length. The InGaAs/Gas QD and InAs/InGaAlAs Qdash SLD samples tested here have active lengths, L, of 500 μm and 600 μm, respectively. In terms of far range peaks, there are no parasitic subpeaks appearing at $2n_{eff}L$, where n_{eff} is the effective refractive index of the optical mode. At this distance, sub-peaks can occur due to Fabry-Perot modulation [1]. The two SLDs tested exhibited low spectral modulation (<0.5dB); a result of effective absorption of photon in the integrated PA section.

InGaAs/GaAs QD and InAs/InGaAlAs Qdash BLDs were tested at 20°C under pulsed current operation (0.4 % duty cycle with a pulse width of 2 μs) at current injections of 2.75 I_{th}, 3.6 I_{th} respectively. To minimize spectral noise, 10 spectral scans were averaged per dataset. To further validate the experimental setup and data acquisition trigger, spectral modulations were compared to fitted data sets based on the input spectrum using a frequency domain version of equation (1) [16]:

$$S_1(\upsilon) = S_o(\upsilon)[1 + V_o \cos(2\pi \frac{OPD}{\lambda})] \quad (3)$$

where $S_1(\upsilon)$ is the spectral interferogram, $S_o(\upsilon)$ is the input spectrum, and V_o is the fringe visibility. The measured data matches well (less than 5% error) with the fit data set for both BLDs.

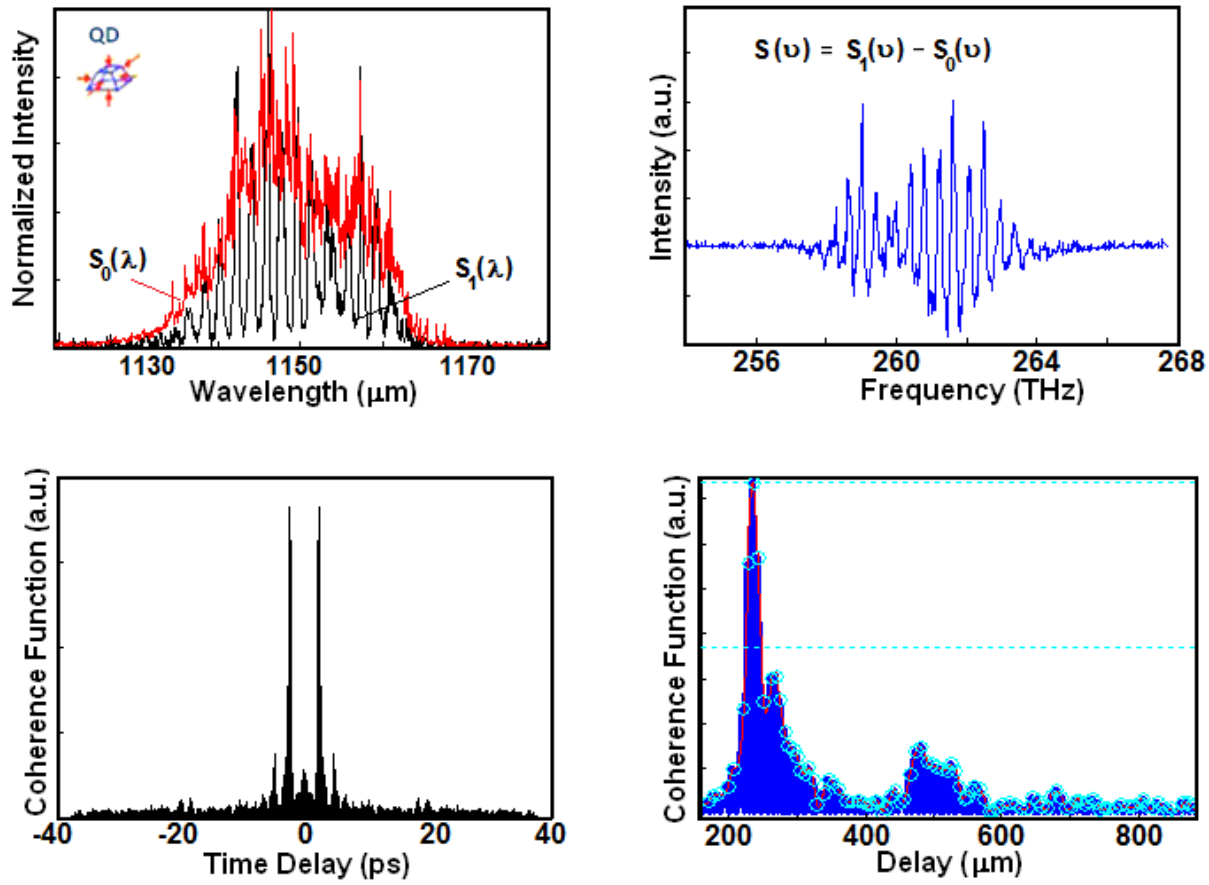

Figure 5. Measured QD BLD source spectrum, $S_o(\lambda)$, and corresponding spectral interferogram, $S_I(\lambda)$, as well as the calculated $S(\upsilon)$ and coherence function in terms of time and distance delay.

The coherence functions were obtained for the InGaAs/GaAs QD BLDs and InAs/InGaAlAs Qdash BLDs with cavity lengths of 800 μm and 600 μm, respectively. Fig. 5 and Fig. 6 illustrate the functions generated from $S_I(\lambda)$ and $S_o(\lambda)$ to yield the temporal coherence functions. The input spectrum ($S_o(\lambda)$) tightly envelopes the spectral interferogram, $S_I(\lambda)$. The coherence function in terms of time delay reveals a slight center peak which corresponds to remnants of the input signal still in the $S(\upsilon)$ function. Theoretically, the l_c in fiber for InGaAs/GaAs QD BLD is 23.05 μm, experimentally it is 22.93 μm; whereas the calculated and measured l_c for the InAs/InGaAlAs Qdash BLD is 48.39 μm and 51.07 μm, respectively. From the measured signals, the l_c in air is 33.48 μm and 74.56 μm, for the QD and Qdash BLDs, respectively. Both short and long range subpeaks in both QD and Qdash BLDs were suppressed to less than 8 and 16 dB, respectively, due to low spectral modulation and spectral dips. As evident from the input source spectrum the Qdash BLD sample had a better signal-to-noise ratio (SNR) which contributes to this difference. These results confirm the Gaussian-like nature of the emission from the naturally inhomogeneous QDs and Qdashes and multiple excitation states. Such spectra generated coherence lengths close (to within 0.5% and 5.5%, respectively) to the theoretical value, which results in less error than other published results [4,7]. The variation may be attributed to spectral phase and amplitude fluctuations of the non-optimized structure. It is worth noting that while producing a high optical power output, the spectral bandwidth of BLD devices can be potentially broadened by employing the chirp of QD/Qdash sheets or spatial bandgap engineering utilizing the quantum nanostructure intermixing [17]. With a few monolithically integrated and intermixed BLDs, high OCT resolution can be achieved.

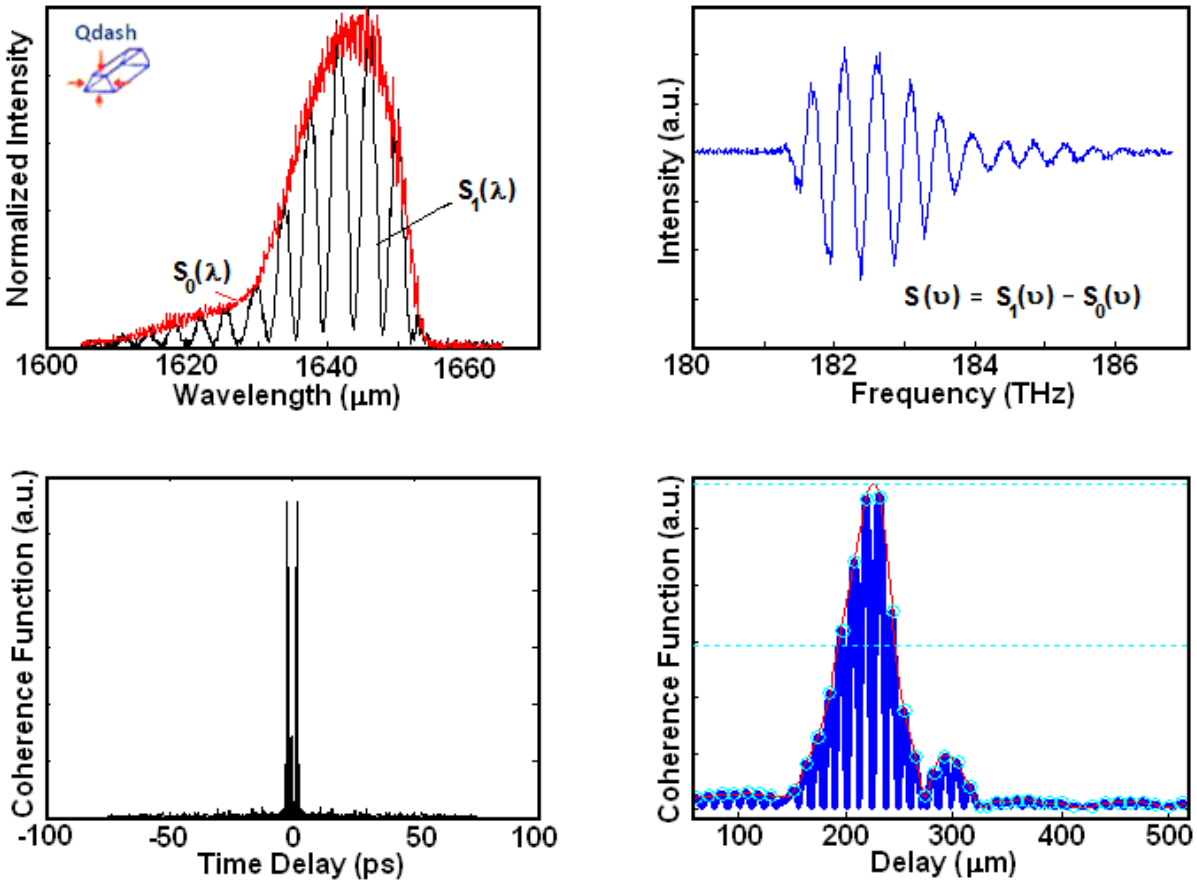

Figure 6. Measured QD BLD source spectrum, $S_o(\lambda)$, and corresponding spectral interferogram, $S_I(\lambda)$, as well as the calculated $S(\upsilon)$ and coherence function in terms of time and distance delay.

5. CONCLUSION

We successfully measured and evaluated the temporal coherence function of QD and Qdash based SLDs and BLDs using a simple optical fiber-based spectral interferometer. In comparing the low coherency of SLDs with BLDs, it is evident that even though BLDs do not produce low ripple spectra compared to SLDs fabricated on similar type of structures, the corresponding coherence function is free of significant sidelobes and subpeaks which would otherwise introduce significant image artifacts and detracted from the axial resolution. Our results confirm that both SLD and BLD based on QD and Qdash nanostructures are promising for low coherent applications such as OCT. The SLDs demonstrated yielded axial resolution in fiber below 3 μm and 10 μm for QD and Qdash based active regions respectively, which would enable valuable epidermal and dental based OCT imaging.

ACKNOWLEDGEMENTS

This work is supported in part by the National Science Foundation (NSF) under Grant No. 0725647, US Army Research Laboratory (ARL), the Pennsylvania Infrastructure Technology Alliance (PITA), a partnership of Carnegie Mellon University, Lehigh University and the Commonwealth of Pennsylvania Department of Community and Economic Development.

REFERENCES

[1] A. F. Fercher, W. Drexler, C. K. Hitzenberger and T. Lasser, "Optical coherence tomography - principles and applications," Rep. Prog. Phys., (66), 239-303 (2003).

[2] J.M. Schmitt "Optical coherence tomography (OCT): a review," IEEE J. of Sel. Topics in Quant. Elect., (5) 1205 - 1215, (1999)

[3] G.A. Alphonse, D.B. Gilbert, M.G.Harvey, and M. Ettenberg, "High-power superluminescent diodes," IEEE J. Quantum Electron, (QE-24), 2454–2457 (1988)

[4] D.S. Mamedov, V.V. Prokhorov, and S.D. Yakubovich, "Superbroadband high-power superluminescent diode emitting at 920 nm," Quantum Electron. (33), 471-473 (2003).

[5] C. E. Dimas, H. S. Djie, and B. S. Ooi, "Superluminescent diodes using quantum dots superlattice," J. Cryst. Growth, (288), 153-156 (2006).

[6] H. S. Djie, C. E. Dimas, and B. S. Ooi, "Wideband quantum-dash-in-well superluminescent diode at 1.6 μm," IEEE Photon. Technol. Lett., (18),1747–1749 (2006).

[7] M. Rossetti, L. Lianhe Li, A. Markus, A. Fiore, L. Occhi, C. Velez, S. Mikhrin, I. Krestnikov, and A. Kovsh,"Characterization and Modeling of Broad Spectrum InAs–GaAs Quantum-Dot Superluminescent Diodes Emitting at 1.2–1.3 μm," IEEE J. Quant. Elect., (43), 676-686 (2007).

[8] B. S. Ooi, H. S. Djie, Y. Wang, C. L. Tan, J.C.M. Hwang, X. M. Fang, J. M. Fastenau, A.W.K. Liu, G.T. Dang, and W.H. Chang "Quantum dashes on InP substrate for broadband emitter applications," IEEE J. Sel. Top. Quantum Electron., (14), 1230-1238 (2008).

[9] H. S. Djie, B. S. Ooi, X. -M. Fang, Y. Wu, J. M. Fastenau, W. K. Liu, and M. Hopkinson, "Room temperature broadband emission of InGaAs/GaAs quantum-dots laser," Opt. Lett., (32), 44-46 (2007).

[10] H. S. Djie, C. L. Tan, B. S. Ooi, J. C. M. Hwang, X. -M. Fang, Y. Wu, J. M. Fastenau, W. K. Liu, G. T. Dang, and W. H. Chang, "Ultra-broad stimulated emission from quantum-dash laser," Appl. Phys. Lett., (91), 111116 (2007).

[11] A. Kovsh, I. Krestnikov, D. Livshits, S. Mikhrin, J. Weimert, and A. Zhukov, "Quantum dot laser with 75nm broad spectrum of emission," Opt. Lett. (32), 793-795 (2007)

[12] Y. Arakawa and H. Sakaki, "Multidimensional quantum well laser and temperature dependence of its threshold current," App. Phys. Lett., (40), 939 (1982)

[13] J. Goodman, Statistical Optics, New York: Wiley, (1985).

[14] H. K. Teng, C. N. Chang and K. C. Lang, "Determination of path length difference by low coherence interference spectrum," Opt. Laser Eng., (42), 437-446 (2004).

[15] K. E. Braun, J. D. Boyer, M. H. Henderson, D. F. Katz, and A. Wax, "Label-free measurement of microbicidal gel thickness using low-coherence interferometry," J. Biomed. Opt., (11), 020504 (2006).

[16] M. Jedrzejewska-Szczerska, R. Bogdanowicz, M. Gnyba, R. Hypszer, and B. B. Kosmowski, "Fiber-optic temperature sensor using low-coherence interferometry," Eur. Phys. J. Special Topics, (154), 107-111 (2008).

[17] C. L. Tan, H. S. Djie, Y. Wang, C. E. Dimas, V. Hongpinyo, Y. H. Ding, and B. S. Ooi, "Wavelength tuning and emission width widening of ultrabroad quantum dash interband laser," Appl. Phys. Lett., (93), 111101 (2008).